27. Fachtagung "Experimentelle Strömungsmechanik"
3. – 5. September 2019, Erlangen

Hydrodynamische Größen- und Dichtefraktionierung von Mikropartikeln im Serpentinenkanal

Hydrodynamic size and density fractionation of microparticles in a serpentine channel

Sebastian Blahout[1], Simon R. Reinecke[2], Harald Kruggel-Emden[2], Jeanette Hussong[1]
[1]AG Lasermesstechnik der Mehrphasenströmungen, Institut für Thermo- und Fluiddynamik, Fakultät für Maschinenbau, Ruhr-Universität Bochum
[2]Fachgebiet Mechanische Verfahrenstechnik und Aufbereitung, Institut für Prozess- und Verfahrenstechnik, Fakultät für Prozesswissenschaften, Technische Universität Berlin

Mehrdimensionale Partikelfraktionierung, APTV, µPIV, Serpentinenkanalströmung
Multi-Dimensional Particle Fractionation, APTV, µPIV, Serpentine Channel Flow

Abstract

In the present study, we investigate the size and density fractionation of microparticles in a sharp corner serpentine channel for different bulk Reynolds numbers. To study the 3D dynamics of the particle motion and the flow, Astigmatism Particle Tracking Velocimetry (APTV) and micro Particle Image Velocimetry (µPIV) measurements are combined. Measurement results are compared to numerical results gained by a Lattice Boltzmann Method (LBM).
Results reveal the existence of four spatially separated particle equilibrium trajectories that merge into two particle equilibrium trajectories beyond a critical bulk Reynolds number. Furthermore, we discover spatially separated equilibrium trajectories for Polystyrene (PS) particles of different diameters, as well as for particles of identical diameter but different relative density (Polystyrene and Melamine). The present study provides a proof of principle for multi-dimensional fractionation of bidisperse microparticle systems in a sharp corner serpentine channel.

Introduction

The availability of microparticles with well-defined, monodisperse properties is important for several industrial branches, such as metallurgy, food industry or chemical industry. Current developments aim to utilize microfluidic devices to fractionate particles with nominal diameters in the order of $O(D_P) \approx 10\,\mu m$ [Zhang et al., 2015, Fan et al., 2014, Dincau et al., 2018]. This is because microfluidic devices show an increased selectivity for these particle sizes compared to conventional fractionation methods.
In-plane separation of microparticles of different sizes is observed in serpentine channels by means of time and depth integrated fluorescence imaging. The spatial separation of different particles and their focus on equilibrium trajectories is supposed to develop due to a combination of secondary Dean vortex flow, particle centrifugal forces and inertial migration of particles [Di Carlo, 2009]. An in-plane particle migration towards different equilibrium trajectories is observed for different particle sizes and densities depending on the bulk Reynolds number.

GALA e.V., Karlsruhe, Germany, ISBN 978-3-9816764-6-4

In the present study, we determine the spatial orientation of particle equilibrium trajectories and the corresponding velocity fields by means of µPIV and APTV [Cierpka et al., 2010]. Measured flow fields are furthermore compared to LBM simulations.
In the course of this paper, we show for the first time that a multidimensional fractionation of microparticles with different size and density may be realised in a sharp corner serpentine microchannel.

Experimental Set-up and Measurement Procedure

Measurements are performed with an EPI-fluorescence microscope (Nikon Eclipse LV100) with an objective lens of M_{Obj} = 20 magnification (20X Nikon CFI60 TU Plan Epi ELWD). The utilized combination of imaging optics results in a total magnification of M = 14. For particle illumination, a double-pulsed, dual-cavity Nd:YAG laser (Litron Nano S 65-15 PIV) is coupled into the microscope. Particle images are recorded with a CCD double-frame camera (LaVision Imager pro SX) controlled by the LaVision software DaVis 8.4. Astigmatism effects of particle images are generated by inserting a cylindrical lens with a focal length of f = 200 mm in front of the CCD camera.
All measurements are performed downstream in the 24th loop of a sharp corner serpentine channel of h = 50 µm height and w = 200 µm width. Different bulk Reynolds numbers Re = $\frac{u_{max} \cdot D_h}{\nu}$ are generated with a volume flow controlled syringe pump (HLL LA-800).
Commercial particles (microParticles GmbH) whose properties are listed in Table 1, are used.

Table 1: Particle properties.

Diameter D_P [µm]	3.55 ± 0.07	9.89 ± 0.10	9.84 ± 0.26
Density ρ_P [gcm^{-3}]	1.05	1.05	1.51
Material	Polystyrene (PS)	Polystyrene (PS)	Melamine (MF)

The flow field is characterised by means of µPIV at different bulk Reynolds numbers. For this, PS tracers with a nominal diameter of D_P = 1.19 ± 0.03 µm are used. In combination with the imaging optics in use, this results in a depth of correlation of z_{corr} = 15 µm [Olsen and Adrian, 2000]. In every measurement set, 300 images are recorded at 26 planes equidistantly located over the channel height with a distance of Δz = 2 µm in between. Before cross-correlation, all images are pre-processed. A subtract time filter over all images of one recording set is used to reduce background noise, e.g. of particles sticking to the ground. To reduce salt-and-pepper noise, a sliding average filter with Gaussian weighting function of 3 pixels filter length is applied. Afterwards, the ensemble averaged cross-correlations are performed with decreasing interrogation window sizes of 96 x 96 pixels and 48 x 48 pixels with 50% overlap.
To determine the bulk Reynolds number regime, at which differently sized particles undergo a transition from two to one visible equilibrium trajectory, fluorescence images are recorded. For this, particle signals are recorded over 1000 double-frame images and the corresponding particle positions are detected.
The three-dimensional reconstruction of particle positions is performed using an APTV approach. Here, 500 images are recorded at three measurement planes, which have a distance of Δz = 15 µm from each other. The measurement depth is found to be always larger than the channel height. APTV recordings are evaluated using a self-written MATLAB code.

LBM

Micro-PIV measurements are prone to systematic errors, due to a finite correlation depth that covers approximately 30% of the channel height in the present study. Therefore, experimen-

GALA e.V., Karlsruhe, Germany, ISBN 978-3-9816764-6-4

tally derived velocity fields are compared against simulation results, which are gained by utilizing a Lattice Boltzmann Method (LBM). LBM stands out through its simplicity in implementation and its great scalability for parallel processing [Aidun and Clausen, 2010].
It is based on so called density distribution functions f, which are associated to the grid nodes $\boldsymbol{r}$ and the discrete velocities e_i. Each simulation step is divided into a propagation step, where all the distribution functions are propagated according to their respective velocities and a collision step, where all the distribution functions arriving at one node collide:

$$|f(\boldsymbol{r}+\boldsymbol{e}_i\Delta t, t+\Delta t)\rangle = |f(\boldsymbol{r},t)\rangle - \Omega(\,|f(\boldsymbol{r},t)\rangle - |f^{eq}(\boldsymbol{r},t)\rangle) + |F\rangle \qquad (1)$$

Here Ω describes the so called collision operator and F an optionally applied volume force.
There are different approaches to implement the collision operator. We use the Multiple Relaxation Time model on a D3Q19 (three dimensions, nineteen velocities) grid as described in [d'Humieres et al., 2002]. To realize the no slip boundary conditions, we use quadratically interpolated bounce back methods as described in [Bouzidi et al., 2001].
In the present study, all numerical results are performed using periodic boundary conditions in x-direction and a spatial resolution of 2 µm/node.

Results and Discussion

In a first step, the Reynolds number region, at which a transition from two to one visible particle equilibrium trajectory takes place, is identified. This region shifts to higher Reynolds numbers with decreasing particle diameter. Figure 1 shows time integrated particle trajectories of particles with diameters D_P = 3.55 µm and D_P = 9.89 µm at bulk Reynolds numbers of Re = 100 and Re = 150. Please note, the overall flow direction takes place in positive x-direction. Here, a transition of particle equilibrium trajectories can be observed for particles of D_P = 9.89 µm.

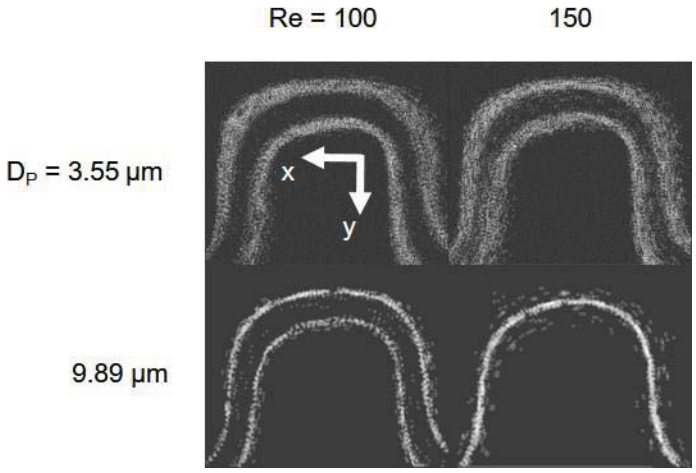

Figure 1: Particle trajectories for particle fractions with D_P = 3.55 µm and D_P = 9.89 µm diameter at bulk Reynolds numbers of Re = 100 and Re = 150.

For a bulk Reynolds number of Re ≥ 150, spatially separated particle equilibrium trajectories can be observed for 3.55 µm and 9.89 µm particles. Therefore, these two particle groups may be successfully fractionated, if a suitable separation of the fluid streams, containing one of both particle groups, is realized downstream the serpentine channel. This will be discussed in more detail later in this section.
To gain a better insight into the dynamics of particle trajectories, the underlying flow field is characterized. For this, µPIV measurements are performed and compared to velocity fields resulting from LBM simulations. Figure 2 a) and b) show measured flow fields taken at half the channel height for Re = 100 and Re = 150. These are compared to the simulated velocity fields in Figure 2 c) and d) at the same channel position and bulk Reynolds numbers.

GALA e.V., Karlsruhe, Germany, ISBN 978-3-9816764-6-4

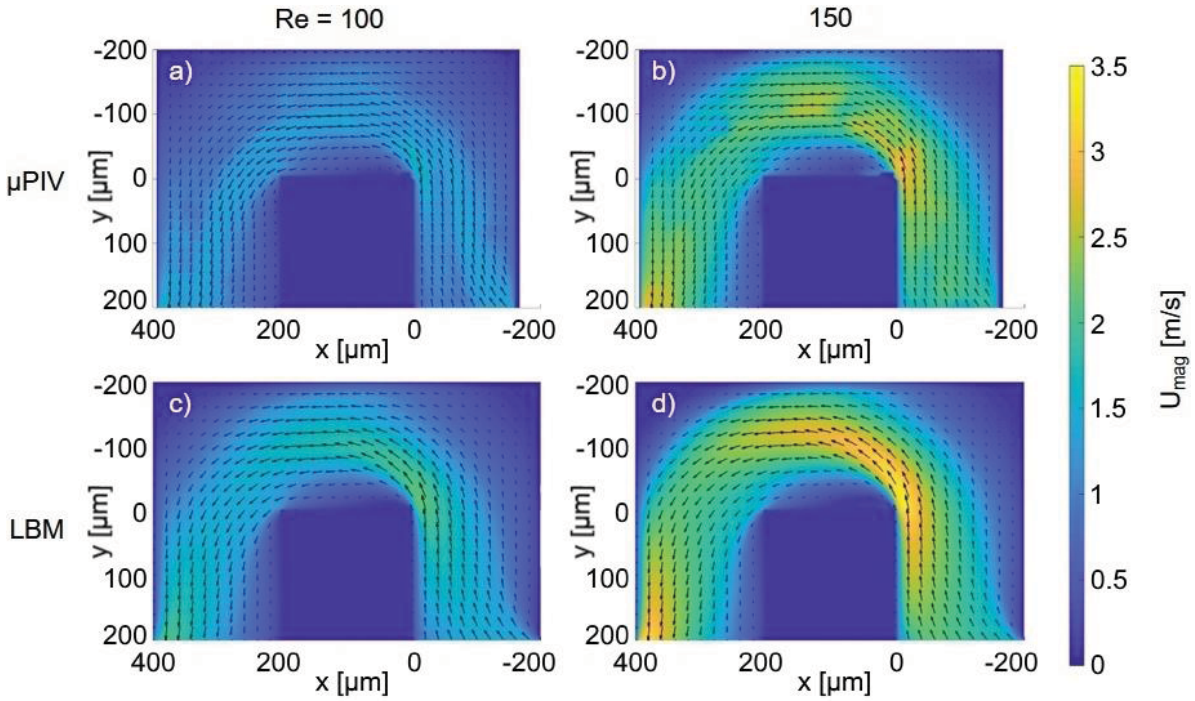

Figure 2: Measured (top row) and simulated (bottom row) velocity fields at bulk Reynolds numbers of Re = 100 (left column) and Re = 150 (right column). In the experimental results of a) and b) only every third and in the numeric results of c) and d) only every tenth vector result over the channel width and height is plotted.

The same characteristic features of the experimentally and numerically obtained flow fields are revealed from these exemplary results. Thus, a sharp rise in velocities can be observed at the leading edge of the inner serpentine wall with rising bulk Reynolds number. We assume that this region plays a key role for the migration dynamics of particles, as acceleration, particle centrifugal forces and shear gradient forces on particles are expected to dominate here. Downstream of the edge, a separation region can be observed. It may be noted, that no particle accumulation was observed in this region.
However, to determine relative motions between fluid and particles, the full 3D flow field and particle trajectories need to be determined. A further comparison of the experimental and numerical results shows, that fluid velocities are underestimated in the experiment. This is assumed to result from a relatively large depth of correlation of z_{corr} = 15 µm present in the µPIV measurements, spanning about 30% of the channel height. To overcome this, the usage of an APTV approach seems to be feasible.

Size fractionation

In the present study we utilize APTV to reconstruct three-dimensional positions of particle groups from two-dimensional recordings. A parameter study was performed to determine the bulk Reynolds number regime at which the best size fractionation results for PS particles with nominal diameters of D_P = 3.55 µm and D_P = 9.89 µm can be expected. For the bulk Reynolds numbers investigated in the present study, best size fractionation results could be achieved at Re = 140. Corresponding 3D particle trajectories gained from APTV results are shown in Figure 3 a) for D_P = 3.55 µm and b) for D_P = 9.89 µm. It is evident, that small particles of D_P = 3.55 µm diameter undergo significant velocity changes of up to 1 m/s while being transported over half a serpentine loop.
In contrast to this, particles of D_P = 9.89 µm nominal diameter move with a relatively constant velocity through the serpentine channel, exhibiting only moderate velocity fluctuations in the order of 0.3 m/s. Furthermore, the smaller particle fraction undergoes stronger oscillations over

GALA e.V., Karlsruhe, Germany, ISBN 978-3-9816764-6-4

the channel height while moving through the serpentine channel. A detailed study on fluid forces acting on both particle groups while moving along their equilibrium trajectories is currently in progress.

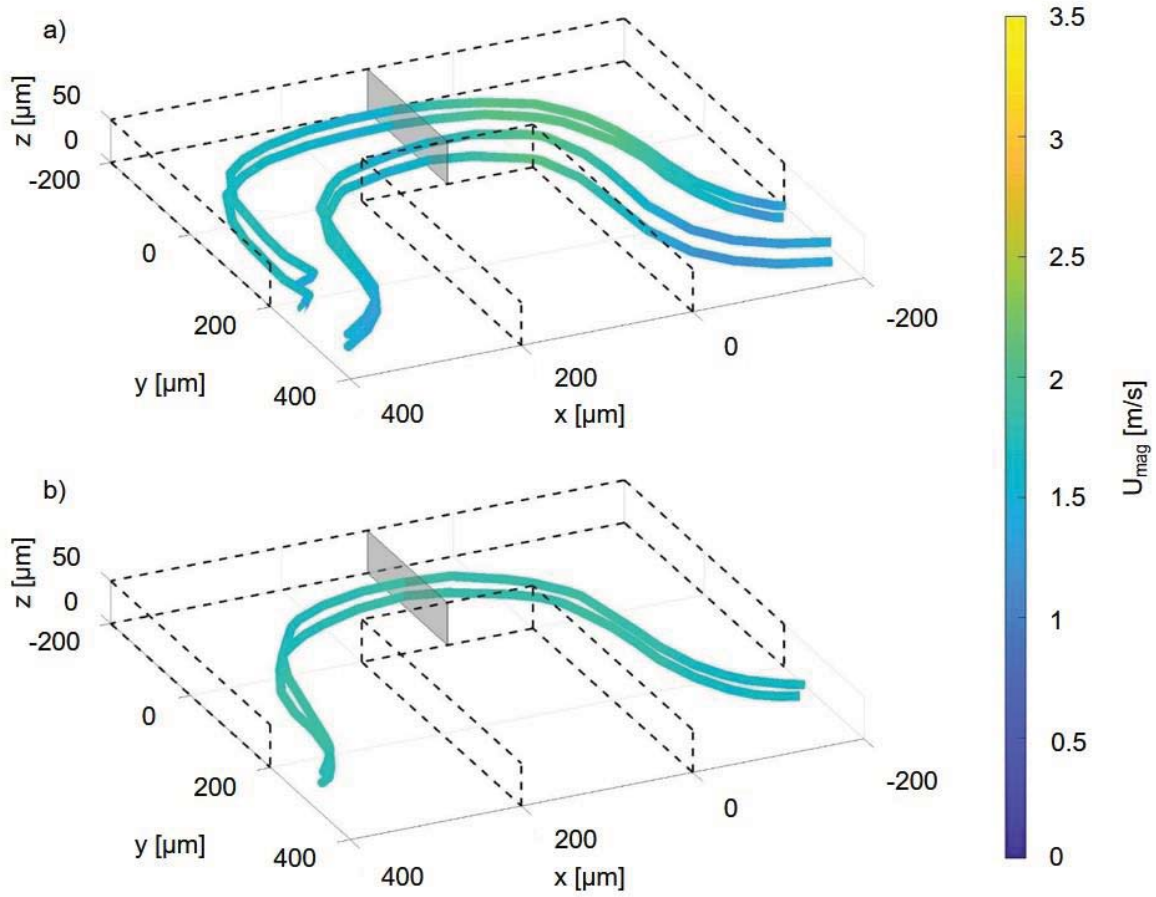

Figure 3: APTV results, showing particle centre line trajectories and velocity magnitudes U_{mag}, at a bulk Reynolds number of Re = 140 of PS particles with nominal diameters of a) D_P = 3.55 µm and b) D_P = 9.89 µm.

Figure 4 a) shows the secondary flow motion at Re = 140 derived from simulations in a cross-section that is labelled in grey in Figure 3 a) and b). In y-direction, only every third vector result is shown. Please note, that due to normalisation and for better visualisation, the axis aspect ratios are unified compared to the real channel dimensions.

Figure 4 a) shows the presence of Dean vortices. Their strength maximizes behind the leading edge (x=y=0) due to a strong acceleration of the flow that is fostered during the switching of the rotation direction of the secondary flow.

The corresponding particle distributions derived from APTV measurements are indicated in Figure 4 b). Here, particles over a volume depth of dx = 200 µm are superimposed. Figure 4 b) reveals that four equilibrium positions of particles emerge in the flow. While a spatial separation of particles along the y-direction is known from literature [Zhang et al., 2015], we show here that a clear separation also occurs over the channel height. However, the distribution of different particle groups appears to be axis symmetric with respect to z/h = 0.35. Therefore, particle fractionation seems feasible only through splitting fluid streams at certain y-positions, for example |y/w| = 0.4 and |y/w| = 0.6 as larger particles (black dots in Figure 4 b) are found near the channel centre between $0.4 \leq |y/w| \leq 0.6$, while smaller particles (red dots in Figure 4 b) accumulate between $0.1 \leq |y/w| \leq 0.2$ and $0.6 \leq |y/w| \leq 0.8$.

GALA e.V., Karlsruhe, Germany, ISBN 978-3-9816764-6-4

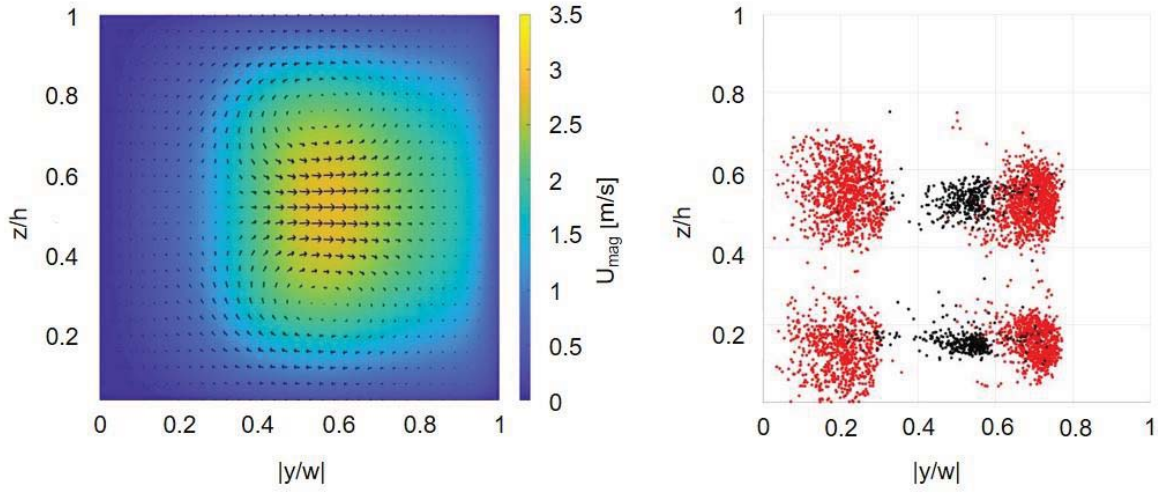

Figure 4: a) Simulated total velocity magnitude and secondary flow normalised with the maximum lateral velocity across the serpentine channel at Re = 140; b) Spatial distribution of Polystyrene particles with D_P = 3.55 µm (red) and D_P = 9.89 µm (black) diameter at Re = 140.

The occurrence of particle equilibrium positions can be also observed in a straight, laminar square duct flow for a bulk Reynolds number of Re = 144 and a channel height to particle radius ratio h/a = 9 [Kazerooni et al., 2017]. Depending on the bulk Reynolds number four or eight particle equilibrium positions may occur in a straight channel flow at the wall bisectors or the channel corners.
Therefore, it is assumed that Dean vortices restrict the number of particle equilibrium positions to four positions. However, further studies are required to better understand how finite particle size effects, referred to as inertial migration effects, and particle centrifugal forces interact to induce different particle equilibrium positions as observed in Figure 4 b).

Density fractionation

While it is known from literature that particles of different sizes may be spatially separated in a sharp corner serpentine channel, we try here for the first time to realize a spatial separation of particles of different densities. Figure 5 a) and b) show sample particle equilibrium trajectories at Re = 110 of PS particles with a nominal diameter of D_P = 9.89 µm and MF particles with a nominal diameter of D_P = 9.84 µm. Please note, that only the centre line trajectories are shown in Figure 5 a). For the actual particle spread over the channel width, refer to Figure 6 b).
Figure 5 a) and b) show, that both particle fractions move with a relatively constant velocity of 1.3 ± 0.2 m/s (PS) and 1.2 ± 0.1 m/s (MF), respectively, through the serpentine channel. This is assumed to be a result from increased inertia of relatively large (Figure 5 a) and additionally relatively dense (Figure 5 b) particle fractions.
Figure 5 a) and b) show that PS particles merge towards four equilibrium trajectories while heavier MF particles assume two equilibrium trajectories. To investigate options of density fractionation, the exact 3D distribution of particles and the underlying flow field must be known. Figure 6 a) shows simulated velocity results at Re = 110 in a cross-sectional plane (as indicated in grey in Figure 5 a) and b). Even though secondary flow motion is also visible here, Dean vortex strength is decreased by about 42%, compared to the case of Re = 140 (see also Figure 4 a).
In Figure 6 b) the distribution of lighter PS particles (black) and denser MF particles (cyan) at Re = 110 is plotted for a flow volume between 0 µm ≤ x ≤ 200 µm. As can be noticed, despite the spatial separation of particle centreline trajectories, displayed in Figure 5 a) and b), both PS and MF trajectories are spread in y-direction.

GALA e.V., Karlsruhe, Germany, ISBN 978-3-9816764-6-4

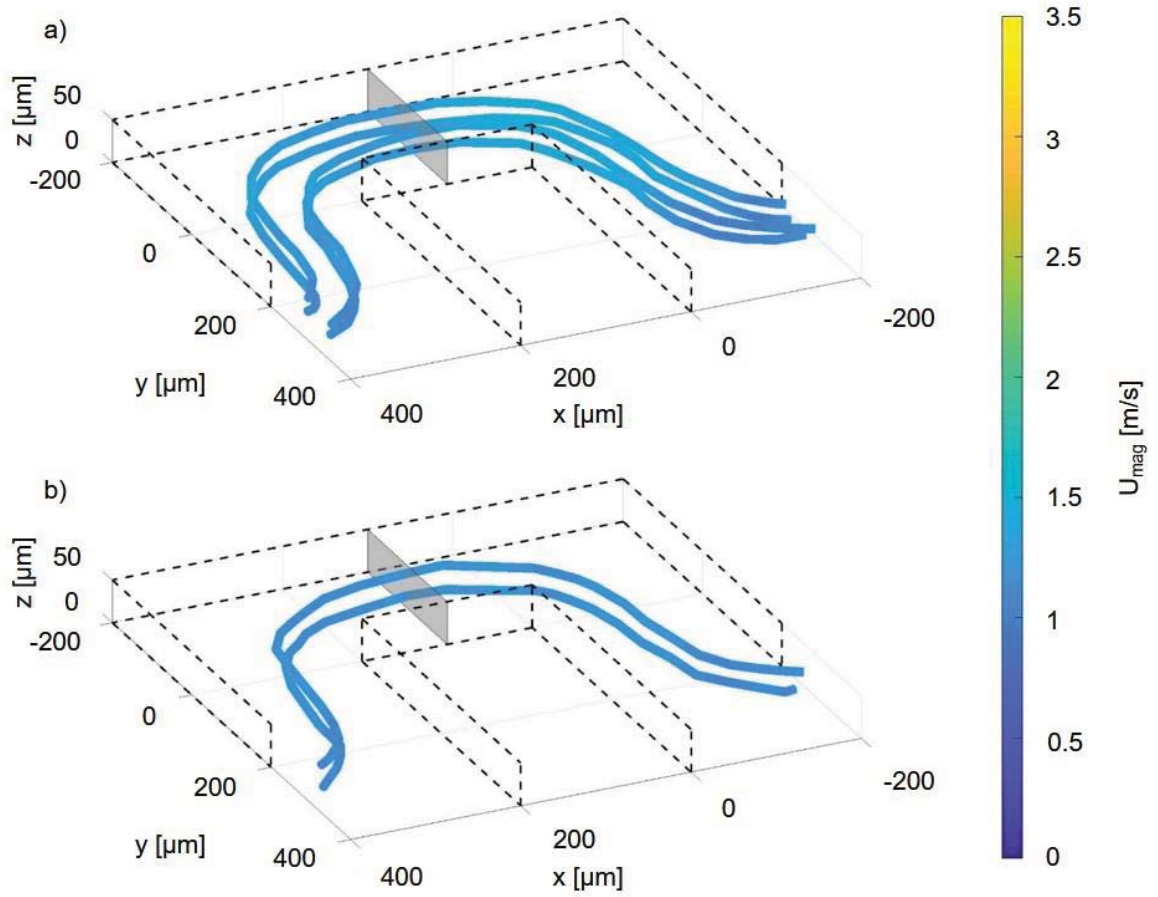

Figure 5: APTV results, showing particle centre line trajectories and velocity magnitudes U_{mag}, at a bulk Reynolds number of Re = 110 of a) Polystyrene (PS) particles of D_P = 9.89 µm diameter and b) Melamine resin (MF) particles of D_P = 9.84 µm diameter.

That is, because PS particles seem to have just started with the transition process from four to two equilibrium trajectories, while MF particles are more advanced in this transition process. A fractionation by splitting fluid streams in y-direction seems possible, when separating particles near the channel centre between 0.4 ≤ |y/w| ≤ 0.6 from particles in the outer channel

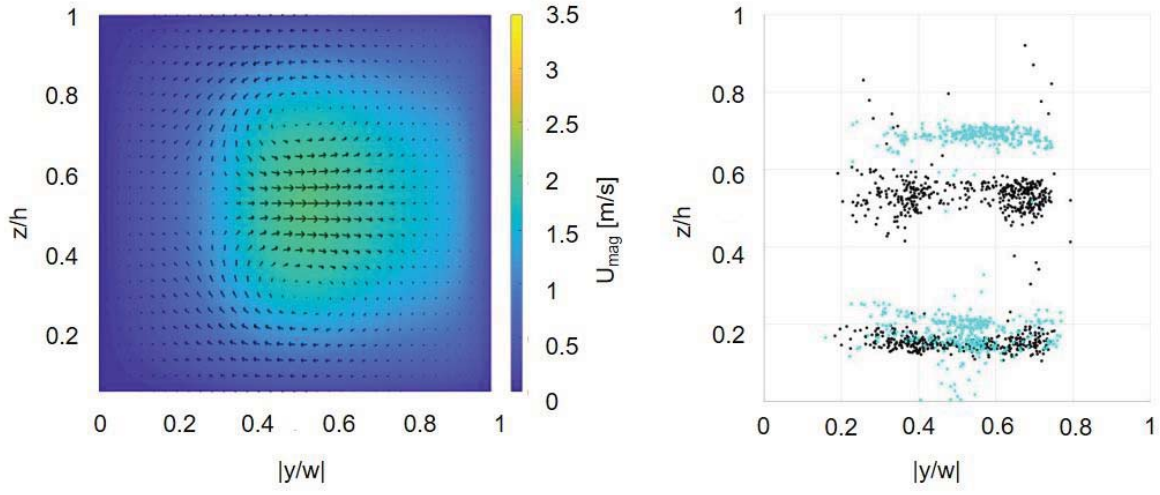

Figure 6: a) Simulated total velocity magnitude and secondary flow normalised with the maximum lateral velocity across the serpentine channel at Re = 110; b) Spatial distribution of polystyrene particles with D_P = 9.89 µm (black) and melamine resin particles with D_P = 9.84 µm (cyan) diameter at Re = 110.

GALA e.V., Karlsruhe, Germany, ISBN 978-3-9816764-6-4

regions. However, a separation of fluid streams over the channel height seems to be suitable in future designs, even though more complex to realize technically.

Conclusion

In the present study, we investigate the capability of a sharp corner serpentine channel to fractionate particles of different sizes and densities for defined particle combinations at different bulk Reynolds numbers. To characterise the flow field, we first performed µPIV measurements and compared the results to LBM simulations. Afterwards, individual particle trajectories were identified by means of APTV.
Up to date, depth-integrated measurements show the existence of one or two particle equilibrium trajectories in lateral channel direction. Here, it is shown for the first time, that spatially separated equilibrium trajectories also evolve over the channel height, leading to a switching between two and four particle equilibrium trajectories.
Particles of different sizes (3.55 µm and 9.89 µm) could be successfully separated, reaching the best fractionation result at a bulk Reynolds number of Re = 140. In the case of density fractionation, a separation of PS and MF particles could be observed at a bulk Reynolds number of Re = 110, although purities of the individual fractions are supposed to be less than in the case of size fractionation. Overall, measurements of 3D particle distributions turn out to be essential for the design of future fractionation devices, as especially for particles with different densities a fractionation over the height might be advantageous.

Acknowledgement

Financial support of the German research foundation (DFG-SPP 2045) is gratefully acknowledged (HU2264/3-1 | KR 3446/14-1).

Literature

Aidun, C. K. and J.R. Clausen. 'Lattice-Boltzmann Method for Complex Flows'. Annu. Rev. Fluid Mech. 42 (2010).
Bouzidi, M., M. Firdaouss and P. Lallemand. 'Momentum transfer of a Boltzmann-lattice fluid with boundaries'. Phys. Fluids. 13 (2001).
Cierpka, C., R. Segura, R. Hain, and C. J. Kähler. 'A Simple Single Camera 3C3D Velocity Measurement Technique without Errors Due to Depth of Correlation and Spatial Averaging for Microfluidics'. Measurement Science and Technology 21, no. 4 (2010).
Di Carlo, D. 'Inertial Microfluidics'. Lab on a Chip 9, no. 21 (2009).
Dincau, B. M., A. Aghilinejad, T. Hammersley, X. Chen, and J.-H. Kim. 'Deterministic Lateral Displacement (DLD) in the High Reynolds Number Regime: High-Throughput and Dynamic Separation Characteristics'. Microfluidics and Nanofluidics 22, no. 6 (2018).
Fan, L.-L., X.-K. He, Y. Han, L. Du, L. Zhao, and J. Zhe. 'Continuous Size-Based Separation of Microparticles in a Microchannel with Symmetric Sharp Corner Structures'. Biomicrofluidics 8, no. 2 (2014).
d'Humieres, D., I. Ginzburg, M. Krafczyk, P. Lallemand and L.-S. Luo. 'Multiple-relaxation-time lattice Boltzmann models in three dimensions'. Philos. Trans. R. Soc. A Math. Phys. Eng. Sci. 360 (2002).
Kazerooni, H. T., W. Fornari, J. Hussong and L. Brandt. 'Inertial Migration in Dilute and Semidilute Suspensions of Rigid Particles in Laminar Square Duct Flow'. Physical Review Fluids 2, no. 8 (2017).
Olsen, M. G., and R. J. Adrian. 'Out-of-Focus Effects on Particle Image Visibility and Correlation in Microscopic Particle Image Velocimetry'. Experiments in Fluids 29, no. 7 (2000).
Zhang, J., S. Yan, R. Sluyter, W. Li, G. Alici, and N.-T. Nguyen. 'Inertial Particle Separation by Differential Equilibrium Positions in a Symmetrical Serpentine Micro-Channel'. Scientific Reports 4, no. 1 (2015).

GALA e.V., Karlsruhe, Germany, ISBN 978-3-9816764-6-4